ME-NETT23 The 23rd Conference of the Mechanical Engineering Network of Thailand

CST-014418

The 23rd Conference of the Mechanical Engineering Network of Thailand
November 4 – 7, 2009, Chiang Mai

A Posteriori Error Estimation for Finite Element Thermal Analysis

Suthee Traivivatana[1] and Pramote Dechaumphai[1,*]

[1] Department of Mechanical Engineering, Chulalongkorn University, Bangkok, Thailand 10330

*Corresponding Author: E-mail: fmepdc@eng.chula.ac.th, Tel: (662) 2186621, Fax: (662) 2186621

Abstract

A posteriori error estimation method for the finite element thermal analysis is presented. The error of heat flux in finite element approximation is determined from the difference between the computed continuous and discontinuous fluxes. The continuous flux is computed by using the flux-based formulation while the standard linear element interpolation functions are used to compute the discontinuous flux. To measure the global error, the L_2 norm error is selected to find the root-mean-square error over the entire domain. In the paper, the finite element formulation and its detailed finite element matrices are presented. Accuracy of the estimated error is measured by the percentage relative error, the ratio between the error and solution norms. Several examples are presented to evaluate the performance and accuracy of the proposed error estimation method.

Keywords*:* Finite Element Method, Thermal Analysis, Error Estimation, Flux-Based Formulation

1. Introduction

The finite element method has been widely used to analyze a large number of engineering problems during the past decades [1,2]. In the prediction of the solutions for the Poisson's equation, the conventional finite element formulation with standard element types is normally employed. The triangular and tetrahedral elements are frequently used in the analysis due to their simplicity in constructing finite element meshes for complex geometry problems. However, the solution accuracy is normally low and may not be acceptable, even though the computational time is saved as compared to the use of the higher-order elements. The solution accuracy may be improved through the use of the *p*-method by increasing or decreesing the orders of the element interpolation functions [2], or the *h*-method of adaptation where the mesh is globally or locally refined or coarsened [3,4].

The objective of this paper is to develop an alternative finite element method to improve the predicted solution of the two-dimensional Poisson's equation. Since the nodeless variable finite elements use the quadratic interpolation functions to express the solution distribution over the element without requiring additional actual nodes, the solution accuracy is increased. In addition,

the paper introduces and applies the flux-based formulation to derive the finite element matrices for the nodeless variable element. Such formulation can simplify the computational effort as compared to the conventional finite element method.

The efficiency of the combined nodeless variable finite element method using flux-based formulation is evaluated by several examples that have exact solutions.

2. Nodeless variable finite element method

2.1 Governing equations and boundary conditions

The Poisson's equation for two-dimensional domain in *x*-*y* coordinate system as shown in Fig. 1 can be written in the conservation form as,

$$\frac{\partial\{E\}}{\partial x}+\frac{\partial\{F\}}{\partial y}=f(x,y) \qquad (1)$$

where $f(x,y)$ denotes the source function. The flux vector components $\{E\}$ and $\{F\}$ contain the heat flux components for thermal analysis or the stress components for structural analysis given by,

$$\{E\}=-c\frac{\partial\{U\}}{\partial x} \text{ and } \{F\}=-c\frac{\partial\{U\}}{\partial y} \qquad (2)$$

where U is the primary variable and c is the material property that depends on types of problem.

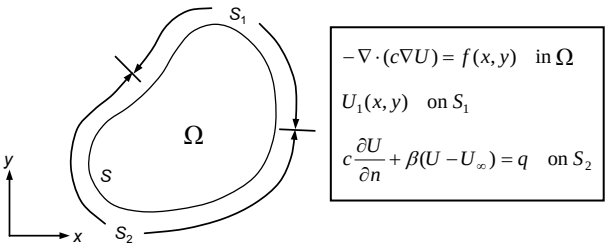

Fig. 1. Two-dimensional domain and boundary conditions for Poisson's problem.

The Poisson's equation shown in Eq. (1) is to be solved together with appropriate boundary conditions that may consist of,

$$U_1(x,y) \quad \text{on } S_1 \qquad (3a)$$

$$c\frac{\partial\{U\}}{\partial n}+d(\{U\}-U_\infty)=q \quad \text{on } S_2 \qquad (3b)$$

where d and U_∞ are constants and q is the secondary variable.

2.2. Nodeless variable flux-based finite element formulation

The flux-based formulation [5,6] is implemented to derive the corresponding finite element equations for a nodeless variable element. For the triangular nodeless variable element, the distribution of the primary variable over the element is assumed in the form,

$$U(x,y)=\sum_{i=1}^{6}N_i(x,y)U_i=\lfloor N(x,y)\rfloor\{U\} \qquad (4)$$

where $\lfloor N(x,y)\rfloor$ consists of the element interpolation functions, and $\{U\}$ is the vector of the unknown primary variables and the nodeless variables. The nodal primary variables are U_1 through U_3, while U_4 through U_6 are the nodeless variables. The element interpolation functions, N_1, N_2, N_3 are identical to the element interpolation functions L_1, L_2, L_3 used for the standard three-node triangular element. The nodeless variable interpolation functions implemented in this paper are,

$$N_4=L_2L_3 \;;\; N_5=L_1L_3 \;;\; N_6=L_1L_2 \qquad (5)$$

Each nodeless variable interpolation function varies quadratically along one edge and vanishes along the other edges. To derive the finite element matrices by means of the flux-based formulation, the method of weighted residuals is first applied to Eq. (1),

$$\int_\Omega N_i\left(\frac{\partial\{E\}}{\partial x}+\frac{\partial\{F\}}{\partial y}-f(x,y)\right)d\Omega=0 \qquad (6)$$

where Ω is the element domain. The Gauss's theorem is then applied to the flux derivative terms to yield,

$$\int_{\Omega} N_i \frac{\partial \{E\}}{\partial x} d\Omega = \int_{S} N_i \{E\} n_x \, d\Gamma - \int_{\Omega} \frac{\partial N_i}{\partial x} \{E\} d\Omega \quad (7a)$$

$$\int_{\Omega} N_i \frac{\partial \{F\}}{\partial y} d\Omega = \int_{S} N_i \{F\} n_y \, d\Gamma - \int_{\Omega} \frac{\partial N_i}{\partial y} \{F\} d\Omega \quad (7b)$$

where S is the element boundary. Substituting Eqs. 7(a)-(b) into Eq. (6) to yield,

$$\int_{\Omega} \frac{\partial N_i}{\partial x} \{E\} d\Omega + \int_{\Omega} \frac{\partial N_i}{\partial y} \{F\} d\Omega = \int_{S} N_i \{E\} n_x \, d\Gamma + \int_{S} N_i \{F\} n_y \, d\Gamma - \int_{\Omega} N_i \, f(x,y) \, d\Omega \quad (8)$$

In the flux-based formulation, the element flux distributions are computed from the actual nodal fluxes as,

$$\{E\} = \sum_{i=1}^{3} \overline{N}_i \{E_i\} = \lfloor \overline{N} \rfloor \{E^n\} \quad (9a)$$

$$\{F\} = \sum_{i=1}^{3} \overline{N}_i \{F_i\} = \lfloor \overline{N} \rfloor \{F^n\} \quad (9b)$$

where $\lfloor \overline{N} \rfloor$ are the standard linear element interpolation functions, i.e., $\lfloor L_1 \quad L_2 \quad L_3 \rfloor$. The $\{E^n\}$ and $\{F^n\}$ are the vectors of the actual nodal fluxes,

$$\{E^n\} = \begin{Bmatrix} -c\lfloor \frac{\partial N}{\partial x} \rfloor \{U\}\big|_1 \\ -c\lfloor \frac{\partial N}{\partial x} \rfloor \{U\}\big|_2 \\ -c\lfloor \frac{\partial N}{\partial x} \rfloor \{U\}\big|_3 \end{Bmatrix}, \{F^n\} = \begin{Bmatrix} -c\lfloor \frac{\partial N}{\partial y} \rfloor \{U\}\big|_1 \\ -c\lfloor \frac{\partial N}{\partial y} \rfloor \{U\}\big|_2 \\ -c\lfloor \frac{\partial N}{\partial y} \rfloor \{U\}\big|_3 \end{Bmatrix} \quad (10)$$

Determination of nodal fluxes depends on the types of problem considered. For heat transfer problem, as an example, the nodal heat fluxes are related to the temperature gradients through the Fourier's law given by,

$$\{E^n\} = \begin{Bmatrix} -k\lfloor \frac{\partial N}{\partial x} \rfloor \{T\}\big|_1 \\ -k\lfloor \frac{\partial N}{\partial x} \rfloor \{T\}\big|_2 \\ -k\lfloor \frac{\partial N}{\partial x} \rfloor \{T\}\big|_3 \end{Bmatrix}, \{F^n\} = \begin{Bmatrix} -k\lfloor \frac{\partial N}{\partial y} \rfloor \{T\}\big|_1 \\ -k\lfloor \frac{\partial N}{\partial y} \rfloor \{T\}\big|_2 \\ -k\lfloor \frac{\partial N}{\partial y} \rfloor \{T\}\big|_3 \end{Bmatrix} \quad (11)$$

Substituting Eq. (10) into Eq. (8), the finite element equations are,

$$[D_x]\{E\} + [D_y]\{F\} = -\{R\} + \{B\} \quad (12)$$

where the matrices $[D_x]$ and $[D_y]$ in Eq. (12) are,

$$[D_x] = \int_A \left\{ \frac{\partial N}{\partial x} \right\} \lfloor \overline{N} \rfloor dA, [D_y] = \int_A \left\{ \frac{\partial N}{\partial y} \right\} \lfloor \overline{N} \rfloor dA \quad (13)$$

and A is the element area. The element nodal vector $\{R\}$ associated with the source variable is,

$$\{R\} = \int_A \{N\} f(x,y) \, dA \quad (14)$$

and the vector $\{B\}$ representing the boundary nodal vector is,

$$\{B\} = \int_S \{N\} \lfloor \overline{N} \rfloor dA (l\{E\} + m\{F\}) = \int_S \{N\} \lfloor \overline{N} \rfloor dA \{q\} \quad (15)$$

where l and m are the components of the unit vector normal to the element boundary. The vector $\{q\}$ appearing in the above Eq. (15) may be replaced by different types of boundary conditions as shown in Eq. (3b). The interpolation functions in Eq. (15) needed for integration along a typical element side s in Fig. 2 are,

$$N_1 = 1 - \frac{x}{L}; \; N_2 = \frac{x}{L}; N_3 = \frac{x}{L}\left(1 - \frac{x}{L}\right) \quad (16)$$

where L is the length of element edge and x is the local coordinate along the edge starting from node 1. The finite element equations, Eq. (12) are derived for all the elements prior to assembling to yield the system equations. Appropriate boundary conditions of the given problem are then applied. Finally, the system equations are solved for the nodal solutions and the nodeless variables.

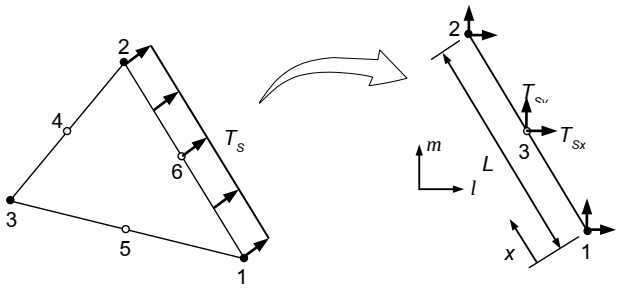

Fig. 2. Discretization of boundary tractions into nodal quantities.

It should be noted that, in solving the same Poisson's equation, the conventional finite element equations are normally appeared in the form [2]

$$[K]\{T\}=\{R\}-\{B\} \tag{17}$$

where the matrices $[K]$, $\{R\}$, and $\{B\}$ are defined by,

$$[K]=\int_A \left(\left\{ \frac{\partial N}{\partial x} \right\} \left\lfloor \frac{\partial N}{\partial x} \right\rfloor + \left\{ \frac{\partial N}{\partial y} \right\} \left\lfloor \frac{\partial N}{\partial y} \right\rfloor \right) dA \tag{18a}$$

$$\{R\}=\int_A f(x,y)\{N\}dA \tag{18b}$$

$$\{B\}=\int_S (\bar{q}\cdot\bar{n})\{N\}dS \tag{18c}$$

3. A posteriori error estimation

3.1 Flux-based formulation for nodal fluxes

Typical heat flux distributions computed by using the conventional finite element formulation for standard three-node triangles are shown in Fig. 3. The computed fluxes are constant and thus discontinuous between elements. Figure 4 shows the concept for continuous flux distributions for same triangular mesh by using the flux-based formulation.

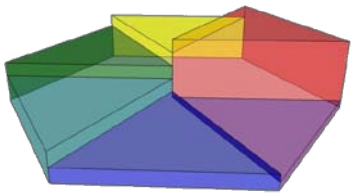

Fig.3 Discontinuous fluxes.

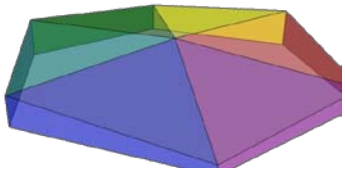

Fig.4 Continuous fluxes.

Errors of fluxes in the conventional finite element approximation are determined from the difference between the computed continuous and discontinuous fluxes. The errors of flux gradients are defined by

$$e_g = g^{FB} - g^{ST} \tag{19}$$

where g^{FB} are flux-based element gradients and g^{ST} are standard element gradients.

The method of weighted residuals is applied to Eq. (19),

$$\int_\Omega [\overline{N}]^T (g^{FB} - g^{ST})\, d\Omega = 0 \tag{20a}$$

or $$\int_\Omega [\overline{N}]^T (g^{FB})\, d\Omega = \int_\Omega [\overline{N}]^T (g^{ST})\, d\Omega \tag{20b}$$

By substituting the element flux distributions from Eq. (9) into the left hand side of Eq. (20b),

$$[M]\{\overline{g}^{FB}\}=[G]\{U\} \tag{21}$$

where $[M]$ is the mass matrix defined by,

$$[M]=\int_\Omega [\overline{N}]^T[\overline{N}]d\Omega \tag{22a}$$

$$[G]=\int_\Omega [\overline{N}]^T \left\lfloor \frac{\partial N}{\partial x_i} \right\rfloor d\Omega \tag{22b}$$

and $\{\overline{g}^{FB}\}$ is the vector of the flux-based nodal fluxes. The finite element equations in Eq. (21) for the thermal analyze is

$$[M]\{\overline{q}^{FB}\}=-k[G]\{\overline{T}\} \tag{23}$$

3.2 Error estimator

To measure the global error, the L_2 norm error is selected to find the root-mean-square error over the entire domain. From Eq. (19), the square of the finite element L_2 norm error for the gradients is

$$\left\| e_g^{FE} \right\|_{L_2}^2 = \int_\Omega (g^{FB} - g^{ST})^2 d\Omega \tag{24}$$

By applying the same concept onto the errors of gradients, the finite element equations for the finite element error square are,

$$\left\| e_g^{FE} \right\|_{L_2}^2 = \lfloor g^{FB} \rfloor [M][g^{FB}] + \lfloor g^{FB} \rfloor [G]\{U\} + \lfloor U \rfloor [K]\{U\} \tag{25}$$

where $[K]$ is the matrix defined by,

$$[K]=\int_\Omega \left\{ \frac{\partial N}{\partial x_i} \right\} \left\lfloor \frac{\partial N}{\partial x_i} \right\rfloor d\Omega \tag{26}$$

The finite element global error for the gradients is computed from

$$\left\| e_g^{FE} \right\|_g = \left[\sum_{element} \left\| e_g^{FE} \right\|_{L_2}^2 \Big/ A_d \right]^{1/2} \quad (27)$$

where A_d is the total domain area. For the problems that has exact solution, the square of exact L_2 norm error for gradients is

$$\left\| e_g^{FB} \right\|_{L_2}^2 = \int_\Omega (g^{EX} - g^{FB})^2 d\Omega \quad (28a)$$

and $$\left\| e_g^{ST} \right\|_{L_2}^2 = \int_\Omega (g^{EX} - g^{ST})^2 d\Omega \quad (28b)$$

where g^{EX} are exact element gradients, $\left\| e_g^{FB} \right\|_{L_2}^2$ is the square of error for flux-based element, and $\left\| e_g^{ST} \right\|_{L_2}^2$ is the square of error for standard element. By applying the same procedure, the exact global error for both flux-based element and standard element are

$$\left\| e_g^{FB} \right\|_g = \left[\sum_{element} \left\| e_g^{FB} \right\|_{L_2}^2 \Big/ A_d \right]^{1/2} \quad (29a)$$

and $$\left\| e_g^{ST} \right\|_g = \left[\sum_{element} \left\| e_g^{ST} \right\|_{L_2}^2 \Big/ A_d \right]^{1/2} \quad (29b)$$

From the concept of measuring discretezation error in the elastic problem which is referred as the Z^2-error estimate [7], the percentage relative error is defined by,

$$\eta = \frac{\|\mathbf{e}\|_{L_2}}{\|\mathbf{u}\|_{L_2}} \times 100 \quad (30)$$

where $\|\mathbf{e}\|_{L_2}$ is the error in the L_2 norm and $\|\mathbf{u}\|_{L_2}$ is L_2 norm of the solution. The mesh adaptation process is terminated when the value of η is less than 5% which is reasonable for many enginee-ring applications [2,7].

4. Numerical examples

To evaluate the performance and accuracy of the combined nodeless variable finite element method with flux-based formulation and the proposed error estimation method, two problems is studied and presented. These problems are: (1) a rectangular plate with specified edge temperature and (2) a square domain with source function.

4.1 Rectangular plate with specified edge temperature

The first example for evaluating the performance of the nodeless variable flux-based finite element method is to solve the Laplace's equation for a rectangular plate. The plate has a specified sine function of temperature along the upper edge as shown in Fig. 5.

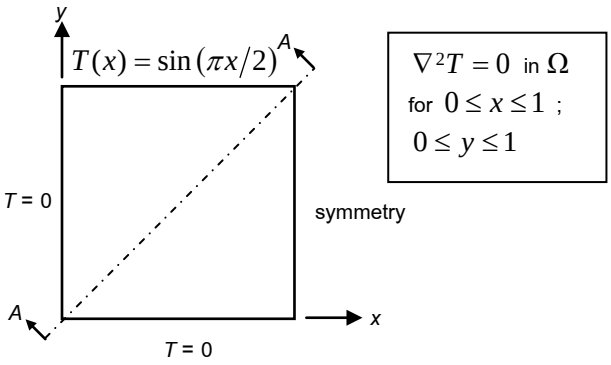

Fig. 5. Problem statement of a rectangular plate with specified edge temperature.

The exact solution for the temperature distribution in the plate is [8],

$$T(x,y) = \frac{\sin(\pi x/2)\sinh(\pi y/2)}{\sinh(\pi/2)} \quad (31)$$

Due to symmetry, only the left-half of the plate is modeled by using four structured finite element meshes. The first mesh (T3NL–M1) with 2 nodeless variable elements (4 nodes), the second mesh (T3NL–M2) with 8 nodeless variable elements (9 nodes), the third mesh (T3NL–M3) with 72 nodeless variable elements (49 nodes), and the fourth mesh (T3NL–M3) with 200 nodeless variable elements (121 nodes) are shown in Fig. 6. The figure also shows the predicted temperature contours obtained from the fourth mesh

model. Figure 7 shows the comparison between the exact solution and the nodeless variable flux-based finite element solution obtained from the fourth mesh model along section *AA*. The L_2 norm and percentage relative errors of the exact global error using the flux-based and standard elements together with the approximate global error are shown in Table 1.

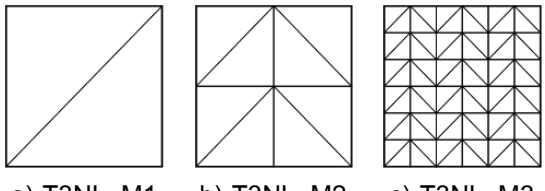

a) T3NL–M1 b) T3NL–M2 c) T3NL–M3

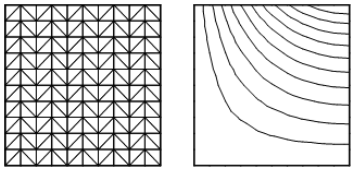

d) T3NL–M4 e) contours

Fig. 6. Structured mesh models and the fourth mesh temperature contours.

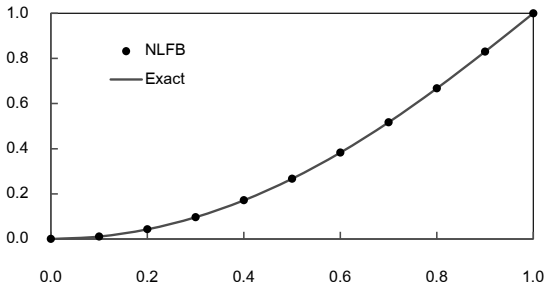

Fig. 7. Comparison between the exact and predicted solutions along section *AA*.

Table 1 Comparisons for global errors of a rectangular plate with specified edge temperature.

Element	$\|e_g^{FB}\|_g$, (η_{FB})	$\|e_g^{ST}\|_g$, (η_{ST})	$\|e_g^{FE}\|_g$, (η_{FE})
T3NL–M1	0.455 (33.28%)	0.527 (36.66%)	0.267 (20.75%)
T3NL–M2	0.182 (16.44%)	0.242 (20.77%)	0.160 (14.55%)
T3NL–M3	0.027 (2.83%)	0.038 (3.90%)	0.026 (2.75%)
T3NL–M4	0.010 (1.02%)	0.013 (1.41%)	0.009 (0.98%)

4.2 Square domain with source function

The second problem is to solve the Poisson's equation with a specified source function. The problem statement of a unit square domain with specified boundary conditions is given in Fig. 8. The specified source function over the plate is [9],

$$f(x,y) = -14x(1-x)(1-2y) - 4y(1-y)(1-2x) + 2(1+2x+7y)[x(1-x)+y(1-y)] \quad (32)$$

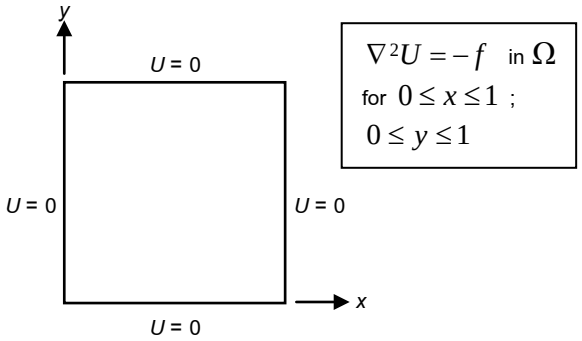

Fig. 8. Problem statement of a unit square domain with specified source function.

The exact solution for the primary variable distribution is,

$$T(x,y) = x(1-x)\,y(1-y)(1+2x+7y) \quad (33)$$

Figure 9 shows the three structure finite element mesh models with 32, 128 and 512 nodeless variable finite elements, respectively. The first T3NL–M1, the second T3NL–M2 and the third T3NL–M3 consist of 25, 81 and 289 nodes respectively. The figure also shows the predicted solution contours obtained from the third mesh model. The comparisons between the exact and three nodeless variable flux-based finite element solutions along the edge x = 0.5 are shown in Fig. 10. The L_2 norm and percentage relative errors of the exact global error using the flux-based and standard elements together with the approximate global error are presented in Table 2.

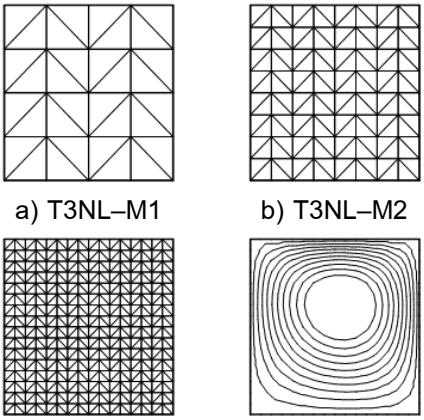

a) T3NL–M1 b) T3NL–M2

c) T3NL–M3 d) contours

Fig. 9. Structured mesh models and the fourth mesh temperature contours.

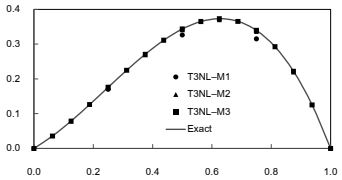

Fig. 10. Comparison between the exact and three finite element solutions along the edge x = 0.5.

Table 2 Comparisons of global errors for a unit square domain with specified source function.

Element	$\left\|e_g^{FB}\right\|_g$, (η_{FB})	$\left\|e_g^{ST}\right\|_g$, (η_{ST})	$\left\|e_g^{FE}\right\|_g$, (η_{FE})
T3NL–M1	0.210 (19.98%)	0.283 (25.20%)	0.190 (19.22%)
T3NL–M2	0.065 (6.96%)	0.089 (9.29%)	0.061 (6.52%)
T3NL–M3	0.018 (1.99%)	0.025 (2.72%)	0.017 (1.88%)

5. Conclusions

The nodeless variable finite element method using flux-based formulation was developed to analyze two-dimensional thermal problems. The nodeless variable finite element and its interpolation functions were described. The flux-based formulation was developed and applied to the nodeless variable finite element to reduce the computational complexity as compared to the conventional finite element method. Performance of the combined procedure was evaluated by using two problems which have exact solutions for comparison. These problems demonstrate that the combined nodeless variable finite element method using flux-based formulation helps increasing the analysis solution accuracy while reducing the total number of unknowns as compared to the conventional finite element method.

6. Acknowledgement

The authors are pleased to acknowledge the Thailand Research Fund (TRF) for supporting this research work.

7. References

[1] Phongthanapanich, S. and Dechaumphai, P. (2006). EasyFEM – an object-oriented graphics interface finite element/finite volume software, *Adv. Eng. Software*, vol.27, 2006, pp. 797 - 804.

[2] Zienkiewicz, O.C. and Taylor, R.L. (2005). The Finite Element Method for Solid and Structural Mechanics, 6th edition, Butterworth-Heinemann, Woburn.

[3] Dechaumphai, P. and Morgan, K. (1992). Thermal Structures and Materials for High-Speed Flight, *AIAA*, Washington, D.C.

[4] Phongthanapanich, S. and Dechaumphai, P. (2004). Evaluation of combined Delaunay triangulation and remeshing for finite element analysis of conductive heat transfer, *Trans. of the CSME*, vol.27, 2004, pp. 319 - 339.

[5] Polesky, S.P., Dechaumphai, P., Glass, C.E., and Pandey, A.K. (1992). Three-dimensional thermal-structural analysis of a swept cowl leading edge subjected to skewed shock-shock interference heating, *J. Thermophys. Heat Transf.*, vol.6(1), 1992, pp. 48 - 54.

[6] Phongthanapanich, S., Traivivatana, S., Boonmaruth, P., and Dechaumphai, P. (2006). Nodeless variable finite element method for heat transfer analysis by means of flux-based formulation and mesh adaptation, *Acta Mechanica*, vol.22(2), 2006, pp. 138 - 147.

[7] Zienkiewicz, O.C. and Zhu, J.Z. (1992). The superconvergent patch recovery and a posteriori error estimates. part 1: The recovery technique, *Int. J. Numer. Methods Engrg.*, vol.33, 1992, pp. 1331 - 1364.

[8] Dechaumphai, P. and Phongthanapanich, S. (2009). Easy Finite Element Method with Software, 1st edition, Alpha Science, Oxford.

[9] Lesaint, P. and Zlamal, M. (1979). Superconvergence of the gradient of finite element solutions, *RAIRO Anal. Numer.*, vol.13, 1979, pp. 139-166